Integrated Seismic and Energy Retrofitting of Masonry Elements Strengthened with PCM-enhanced GTRM/FRCM systems

Abbas FathiAzar[1], *Mahdi* Zanjani[1], *Ignacio* Peralta[2], *Serena* Cattari[1], *Silvia* De Angeli[1], *Victor* Fachinotti[2], *Antonio* Caggiano[1], and *Sergio* Lagomarsino[1*]

[1]DICCA, University of Genoa, Italy
[2]CIMEC, CONICET, Universidad Nacional del Litoral, Santa Fe, Argentina

Abstract. The integration/combination of seismic and energy retrofit measures has been a subject of study for the past decade, exhibiting promising prospects. The main objective of these interventions is to mitigate seismic vulnerability while concurrently enhancing the energy performance and efficiency of new and existing buildings. Integrated approaches can hold the potential for substantial cost savings, time efficiency, and minimal disruption to occupants. The current body of literature emphasizes exploring the benefits of incorporating innovative methods/materials into conventional uncoupled retrofit initiatives. This study focuses on evaluating integrated measures at the panel scale for the prevalent Unreinforced Masonry (URM) typologies in Italy. A design framework has been introduced, aimed at enhancing the seismic capacity of buildings while concurrently improving energy efficiency through the integration of new materials (e.g., highly latent thermal energy storage systems achieved through the integration of Phase Change Materials - PCMs) into retrofit materials. To assess the reduction of the seismic vulnerability, the improvement of the shear strength is estimated by modifying the failure domains, while energy efficiency and thermal-energy storage enhancements are evaluated by using enthalpy-based theories, implemented into open-source software (i.e., FEM-based and through EnergyPlus). Thus, the design variables are those defined by the URM typologies, the adopted retrofitting technique, and the considered envelope. The adopted integrated (seismic and energy retrofitting) solutions will be compared with the standard reference one in terms of the energy consumed by the enclosed building to keep the indoor thermal comfort which also guarantees the target level of structural performance.

1 Introduction

During the past few decades, the construction landscape in Europe has been experiencing a notable shift in focus, moving away from constructing new buildings to prioritizing the

* Corresponding author: sergio.lagomarsino@unige.it

These proceedings are published with the support of EuLA.

improvement of existing ones. This change is driven by two main factors: the aging infrastructure across Europe and the urgent need for environmental sustainability within the built environment. Many buildings in Europe are very old and have reached the end of their intended lifespan showing several potential structural vulnerabilities. These vulnerabilities become even more important in areas prone to earthquakes. On the other hand, European laws emphasize energy-saving measures in buildings to enhance occupant well-being and reduce overall environmental impact [1].

Considering these vulnerabilities and the fact that the existing buildings are significant contributors to energy consumption and carbon emissions [2], retrofitting initiatives emerge as vital solutions. In past years, renovation endeavors and policies have been primarily focused on enhancing the energy efficiency of buildings, often overlooking their structural vulnerabilities which may yield short-term advantages, such as decreased heating/cooling expenses. However, this approach could prove inadequate, particularly in seismic-prone areas, where building damage during seismic events can render the investments in energy retrofitting wasted. On the other hand, solely incorporating seismic retrofitting interventions could potentially compromise the ambitious goal of achieving climate neutrality by 2050. Therefore, there has been an argument in the literature that a successful and cost-effective retrofitting intervention, needs a comprehensive approach that addresses these two issues simultaneously. In line with this, researchers have been exploring and demonstrating the benefits of integrating seismic and energy retrofits [3–5], with some proposing innovative methods [6–8].

These studies mainly focused on combining intervention measures by layering elements and methods for seismic and energy retrofits. In this study, we propose leveraging the properties of Phase Change Materials (PCMs) to integrate seismic strengthening materials. Incorporating PCMs into porous carriers of construction materials has gained interest for enhancing energy efficiency in new and existing buildings [9,10]. PCMs, with their high Thermal Energy Storage (TES) capacity in the form of latent heat, can significantly improve thermal properties, making buildings more sustainable, environmentally friendly, and capable of passive energy improvements [11,12].

Specifically, we suggest incorporating PCM into the mortar used in some seismic strengthening like Textile-Reinforced Mortars (TRMs) or Fiber-Reinforced Cementitious Matrix (FRCM) as these methods have shown promising prospects in intervention projects. This approach offers a cost-effective way to reduce structural vulnerability while simultaneously improving energy efficiency.

To demonstrate our point, we have used a simplified approach by employing an analytical procedure for calculating the strength of a masonry pier both in As-Built and strengthened states. For the energy part, an enthalpy-based approach is solved to accurately analyze the above-mentioned phenomena. The model has been validated by assessing 5 different wall scenarios (URM, URM with single and double TRM/FRCM layer, and URM with single and double PCM-TRM/FRCM layer) and one virtual location in Genova, Italy.

2 Seismic strengthening

When it comes to retrofitting masonry buildings, there are several methods that can be utilized. Among modern solutions addressed to increase the structural capacity of masonry walls, in the past the most used methods were concrete overlays or Fiber-Reinforced Polymer (FRP) overlays, however in recent years the adoption of TRMs and FRCM for retrofitting is on the rise, representing a promising alternative to FRP methods due to their ability to mitigate the shortcomings of FRPs [13,14]. This stems from the substitution of epoxy resins, inherent in FRPs, with mortars in the TRM/FRCM approach. These mortars exhibit better compatibility with the substrate material and are comparatively more cost-effective than

resins. While TRMs and FRCMs are typically distinguished as separate methods in some studies, this paper discusses them within the same framework. TRM/FRCM composites offer a diverse range of applications, incorporating various fiber types—both synthetic and natural—embedded within different inorganic matrices, such as cementitious-based or lime-based materials. These composites can be utilized in different strengthening configurations, including symmetric or asymmetric layouts. Generally, in these methods, a textile overlay, created by high-strength fiber rovings, is externally bonded to masonry walls (either one or both faces) using inorganic matrices like cement- or hydraulic-lime-based mortars. The final thickness of these methods typically ranges from less than one to a few centimeters, along with substrate leveling, often achieved using the same matrix material [15,16]. This method can be used to enhance the seismic performance of both reinforced concrete (RC) and masonry buildings [17–21] and has great potential to be integrated with energy improvements [6,22–24].

Key improvement mechanisms that these methods can bring about include increasing the in-plane bending and shear capacity of masonry piers and spandrels [25,26], and improving the out-of-plane bending capacity [27], especially evident when jacketing both faces of the wall. The efficacy of these methods heavily relies on the force transfer mechanism between the substrata wall and the overlay as well as the fabric and matrix.

2.1 Code-based calculation of strength

To provide context for the analytical approach that is used in this paper, a concise overview of the key features of the Italian guidelines for FRCM composites (CNR DT 215/2018) [28] is provided first. This guideline establishes acceptance criteria for FRCM materials and design regulations for strengthening existing structures.

The guideline also imposes some limitations on FRCM systems. The total weight of organic components, excluding any surface coating, cannot exceed 5% of the inorganic binder weight (cement/lime). The design value of a generic property of the FRCM system is calculated according to Equation 1:

$$X_d = \eta \frac{X_k}{\gamma_m} \tag{1}$$

where η is a conversion factor (0.9 for internal, 0.8 for external, and 0.7 for aggressive environments), X_k is the characteristic value of the property considered and γ_m is the corresponding partial safety factor: γ_m= 1.5 for the Ultimate Limit State (ULS) and γ_m = 1.0 for the Serviceability Limit State (SLS) please note that The design of strengthening interventions of masonry elements shall be carried out only with respect to the ultimate limit state.

2.2 Materials' elastoplastic stress-strain behavior

Since the purpose of this paper is a preliminary evaluation of the advantages and trade-offs of integrated strengthening measures, material properties of existing masonry are assumed as a possible value, however, it is advisable that material properties such as compressive and tensile strength, elastic modulus in compression, and shear strength of existing masonry be determined by in-place tests or laboratory tests of extracted samples.

The stress-strain relation for masonry is defined by an elastic–perfectly plastic relation and no-tensile resistance (EPP-NTR) as shown in Fig. 1(a) which can be characterized by one strength $f_m = 2.4\,MPa$ and two strain values $\bar{\varepsilon}_m = 0.002$ and $\varepsilon_{mu} = 0.0035$. It is worth mentioning that this stress-strain relation doesn't hold in the case of spandrels where the interlocking between masonry units can result in some tensile resistance [29].

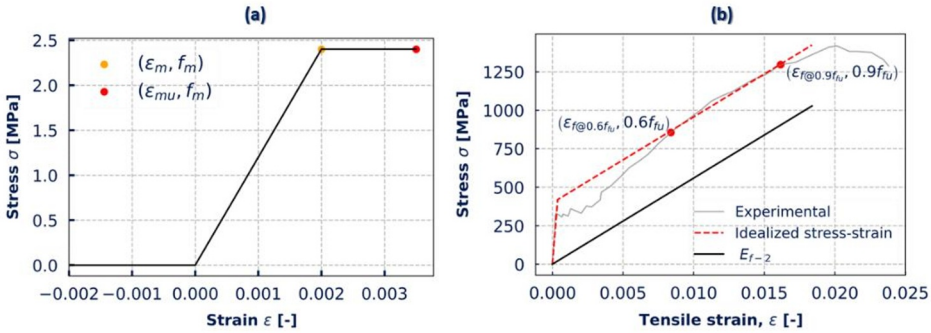

Fig. 1. (a) Stress-strain relationships for masonry; (b) Experimental and idealized stress-strain response of a carbon FRCM.

When subjected to a uniaxial tensile test, FRCMs demonstrate a complex stress-strain response. This behavior is typically represented by a three-branched curve, which delineates the material's response across distinct stages [30,31]:

- Uncracked Stage (Initial Linear Branch): In the initial phase, the FRCM acts as a unified composite.
- Crack Development (Transitional Branch): As the tensile load continues to rise, tiny cracks begin to form and propagate within the matrix. This stage is characterized by a gradual decrease in stiffness, reflected by a flattening of the curve's slope.
- Cracked Stage (Final Linear Branch): Once significant cracking occurs, the matrix loses its effectiveness in transferring load between the fibers. The primary load-carrying capacity rests on the fibers themselves. This final stage exhibits a relatively constant stiffness on the curve until the composite reaches its ultimate tensile strength.

Since the actual stress-strain response of FRCMs is a complex nonlinear behavior, analyzing it can be computationally demanding. Therefore, this study adopts a simplified approach similar to the ACI 549 recommendation [32]. It approximates the complex behavior with a bilinear curve (see Fig. 1(b), red dashed line for an example of the procedure). This idealized curve consists of two straight lines that capture the essential aspects of the material's response:

- The first line represents the uncracked stage, with a slope of E_{f-1}. It ends at the point where the first significant crack appears in the matrix. This is the critical zone where the presence of PCM is expected to have the most significant influence. While more detailed experimental data across all ranges of FRCM behavior would enhance our understanding of the strengthened wall's performance under various strain conditions, this paper focuses on the assessment of the strengthened pier at the ultimate limit state. This state is very close to the ε_{lim} (or σ_{lim} for that matter) values. At these strain levels, the loads are primarily carried by the fabric.
- The second line signifies the cracked stage, characterized by stiffness E_{f-2}. This line is drawn between points corresponding to 0.6 and 0.9 of the ultimate tensile strength (see Equations 2 and 3). Since these points primarily depend on fiber properties, the impact of PCM at this stage can be considered negligible:

$$E_{f-2} = \frac{0.9f_{fu} - 0.6f_{fu}}{\varepsilon_{f@0.9ffu} - \varepsilon_{f@0.6ffu}} \quad (2)$$

where $\varepsilon_{f@0.9ffu}$ and $\varepsilon_{f@0.6ffu}$ are the tensile strain associated with$0.9f_{fu}$ and $0.6f_{fu}$ respectively. The ultimate tensile strain ε_{fu}, is:

$$\varepsilon_{fu} = \varepsilon_{f@0.6ffu} + \frac{0.4 f_{fu}}{E_f} \quad (3)$$

PCM inclusion can have two effects: 1) reduced tensile stress and strain, during the initial uncracked stage, PCM can lower the tensile stress and strain experienced by the composite. This is particularly important because it influences both stiffness and the initiation of cracks; 2) Weakened Bonds, PCM addition can also weaken the bond between the fabric reinforcement, the matrix, and the substrate to which the FRCM is applied. It is worth mentioning that the design of strengthening interventions for masonry elements shall be carried out only considering the ultimate limit state. The behavior of FRCM/TRM in this state is mainly characterized by fabric properties and the only parameter that might manifest itself in the final results will be the conventional strain limit that will be elaborated in the next subsections. In this paper, due to a lack of experimental data, the mechanical influence of incorporating PCM into the FRCM matrix is not considered.

2.3 In-plane shear and flexural capacity at panel scale

The ultimate strength of a pier is influenced by the interaction between its flexural and shear capacities. Higher shear strength allows the pier to withstand greater shear forces before experiencing flexural failure. Conversely, piers with lower shear strength will fail in shear before reaching their full flexural capacity. These failure modes can be individually assessed and then analyzed for their combined effects. In Fig. 2, this interaction is illustrated where the equivalent moment derived from the pier's shear capacity is compared against its moment-curvature relationship. The intersection of the equivalent shear moment line with the moment-curvature curve determines the point at which the pier will fail in shear. For instance, for unstrengthened pier (AB URM) where the dashed red line intersects the moment-curvature curve, signifying shear failure at this specific conditions.

Although the Italian building code NTC18 [33] recognizes various shear failure mechanisms and assigns corresponding shear strengths to each, the CNR DT 215/2018 focuses solely on diagonal tensile failure. The total capacity of the strengthened wall is calculated by combining the shear strength of the un-strengthened wall and the contribution of the FRCM. The former can be calculated using the formula for diagonal cracking failure by Turnšek and Cačovic [34].

$$V_t = l \cdot t \cdot \frac{f_{td}}{b} \cdot \sqrt{1 + \frac{\sigma_o}{f_{td}}} \quad (4)$$

where $b = h_{p,eff}/B_p$ is the pier aspect ratio that should be between 1 to 1.5, f_{td} is the masonry tensile strength, and σ_o is the compressive vertical stress on the pier.
The additional strength provided by the FRCM composite, denoted by $V_{t,f}$. This contribution is calculated using Equation 5:

$$V_{t,f} = \frac{n_f \cdot t_{Vf} \cdot \ell_f \cdot \alpha_t \cdot \varepsilon_{fd} \cdot E_f}{2} \quad (5)$$

where 2 is a safety factor; n_f is the total number of FRCM layers; t_{Vf} is the equivalent thickness of a single FRCM layer; ℓ_f is the size of the FRCM system measured perpendicular to the shear force direction (It's important to note that ℓ_f cannot exceed the wall's width); α_t accounts for the reduced effectiveness of fibers under shear stress; ε_{fd} is the design value for

the maximum strain the fibers can experience. It's typically assumed to be a conventional strain value calculated using the following formula:

$$\varepsilon_{f,d} = \frac{\sigma_{\lim,conv}}{E_f} \tag{6}$$

Flexural strength of both un-strengthened and strengthened piers is computed using their moment-curvature relations that were calculated using the material stress-strain behavior (explained in section 2.2 and demonstrated in Fig. 1) and incorporating the following assumptions:

1- The flexural capacity of the pier is determined by either the compressive failure of the masonry toe when the masonry reaches its compression strain limit ε_{mu}, or the tensile fracture of the FRCM when it reaches its tensile strain limit $\varepsilon_{t,lim}$.
2- The pier is considered homogeneous and isotropic.
3- Since thin masonry piers are being considered, where the thickness is significantly smaller than the in-plane dimensions, the presence of a plane stress field is adopted.
4- Furthermore, plane sections are assumed to remain plane during the whole range of loading.

3 Results and discussion of seismic interventions

For demonstration purposes, the analysis has been conducted on a simple pier with a height of 3 meters, a base of 1.5 meters, and a thickness of 28 centimeters. The wall is constructed from tuff masonry with a unit weight of 20 kN/m³ and a compressive strength of 2.4 MPa. The reinforcement used is Glass Textile Reinforced Mortar (GTRM), which has an equivalent thickness of 0.06 mm and a modulus of elasticity of 200,000 MPa. The Moment-Curvature (M-φ) and M-N domain performance of unstrengthened and strengthened pier are illustrated in Fig. 2 and Fig. 3 respectively. For the unstrengthened pier, strength, and deformation capacity are often dominated by diagonal tension failure. However, when the FRCM system is incorporated, the behavior shifts to flexural behavior, resulting in increased deformation and strength capacity (which later manifests itself in shear-drift behavior).

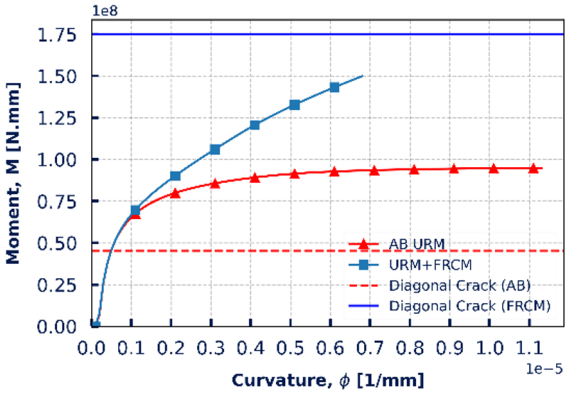

Fig. 2. Moment-Curvature of both unstrengthened (denoted by AB) and strengthened pier (denoted by FRCM).

It is worth noting that this change in behavior is influenced by the pier's aspect ratio (height-to-length ratio) and the acting axial load, which can vary in different locations within a building and during seismic loading. Regarding the aspect ratio, compared to the results presented in Fig. 3, with an aspect ratio of 2, when the aspect ratio increases to greater than

6, the failure mode of both unstrengthened and strengthened piers becomes flexural. However, the strength capacity of the strengthened pier decreases from 139 kN.m to 64 kN.m. The aspect ratio of 6 however is very uncommon in ordinary URM buildings. In contrast, for an aspect ratio of 1, the governing failure modes for both unstrengthened and strengthened piers remain the same as before, while the capacity of the strengthened pier increases from 139 kN.m to 252 kN.m.

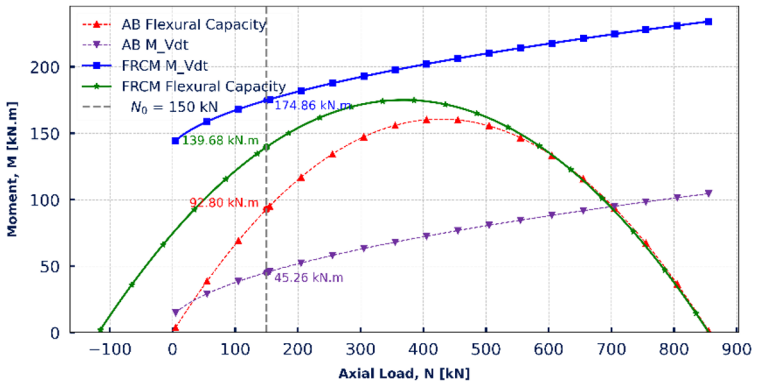

Fig. 3. M-N domain performance of both unstrengthened (denoted by AB) and strengthened pier (denoted by FRCM).

In addition to the increase in strength, the strengthened pier will have a higher deformation capacity. The common approach to calculating shear-drift law for unstrengthened piers is using the procedure presented in CNR-DT 212/2013 [35] which defines specific displacement ranges (denoted as θ_{DL-i}) corresponding to various damage states defined in line with EMS98 [36], along with the strength reduction (referred to as β_{DL-i}) that is happening with increasing displacement from one damage state to the next. Table 1 shows the drift and the residual resistance ranges for different damage states. In general, according to EMS98, in DS3, categorized as moderate damage, structures exhibit significant cracks in walls and may experience partial collapse of non-load-bearing walls. DS4, indicating severe damage, involves partial collapse of load-bearing walls or significant structural deformation. DS5 signifies near total or total collapse of the structure, leading to complete loss of structural integrity, rendering the building uninhabitable and potentially necessitating demolition.

Table 1. Drift and the residual resistance ranges for different damage states (as per CNR-DT 212/2013 [35]).

Pier	Drift [%]			Residual resistance [-]	
	$\boldsymbol{\theta_{DS3}}$	$\boldsymbol{\theta_{DS4}}$	$\boldsymbol{\theta_{DS5}}$	$\boldsymbol{\beta_{DS3\rightarrow4}}$	$\boldsymbol{\beta_{DS4\rightarrow5}}$
Flexural behavior	0.4-0.8	0.8-1.2	1.2-1.8	1	0.8-0.9
Shear behavior	0.25-0.4	0.4-0.6	0.6-0.9	0.6-0.8	0.25-0.6

In cases where there is probability that the flexural and shear failure mechanisms interact the drift and residual resistance values associated with different levels of damage can be calculated using Equation 7.

$$\theta_i = \begin{cases} \theta_{i,FL} & V_{pf}/V_{dt} < 0.95 \\ \theta_{i,FL} - 4(\theta_{i,FL} - \theta_{i,SH}) * (V_{pf}/V_{dt} - 0.95) & 0.95 \leq V_{pf}/V_{dt} \leq 1.2 \\ \theta_{i,SH} & V_{pf}/V_{dt} > 1.2 \end{cases} \quad (7)$$

where the V_{pf} *and* V_{dt} are shear capacity of the pier due to flexural and diagonal shear failure mechanisms respectively.

In the case of the strengthened pier, experimental findings in the literature indicate that the contribution of FRCM primarily starts after masonry cracking [37,38]. Consequently, the initial stiffness and cracking point are anticipated to remain relatively consistent. The concept of pseudo-ductility can be used in estimating potential increases in corresponding displacements. Pseudo-ductility is defined as the ratio of ultimate displacement to the displacement at cracking. These values typically can be derived from experimental tests. Ref. [26] provides a concise overview of such studies and their reported pseudo-ductility values which in the case of tuff masonry ranges from 2.4 to 2.7 [39–41]. Considering that the displacements associated with cracking remain relatively same for both unstrengthened and strengthened piers, the increase in Pseudo-ductility can approximately translate to an increase in displacement at the damage state. However, it is important to note that this increase is not straightforward. The strengthened pier might exhibit a different failure mode, which can significantly alter the shape of the backbone curve.

4 Energy retrofitting: URM and PCM-TRM/FRCM wall scenarios

4.1 Materials and components

The following cases (Fig. 4) are analysed:

- **Scenario a** - reference URM: of 280 mm thickness made of mortar + tuff stones having an hogenized density ρ = 2000 kg/m^3, a specific heat capacity C_p = 1165 J/kgK and a thermal conductivity λ = 0.466 W/(m K).
- **Scenario b-c** URM+GTRM: Reference URM as in scenario a + 15 mm of (one or two layers) Glass Textile Reinforce Mortar (GTRM) with a density ρ = 2250 kg/m^3, specific heat capacity - Cp = 845 J/kg×K, thermal conductivity λ = 0.780 W/(m×K)).
- **Scenario d-e** URM+FRCM: as in scenario b-c + RT RT24HC RUBITHERM® PCM (Fig. 5): Heat Storage Capacity = 200 J/g, melting area of 23-26 °C and 20% Vf (%) within the mortar of the GTRM layer.

Table 2 provides the key TES parameters and thicknesses, while Fig. 4 shows the main sketches and the cases to be analysed.

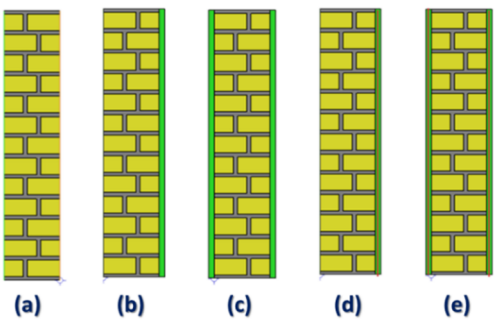

Fig. 4. (a) URM, URM with (b) single and (c) double FRCM layer and URM with (d) single and (e) double PCM-FRCM layer. In all cases, no thermal insulation package (i.e., neither external nor internal layers) has bee provided, as these simulations are a comparative academic exercise.

Table 2. Overview parameters for the 5 wall scenarios.

	URM	GTRM-layer	RT24HC
Density [kg/m^3]	2000	2250	800 (S) / 700 (L)
Specific heat capacity (C_p) [J/(kg×K)]	1165	845	2000
Thermal conductivity (λ) [W/(m×K)]	0.466	0.780	0.200
Thickness [mm]	280	15	20% in volume fraction

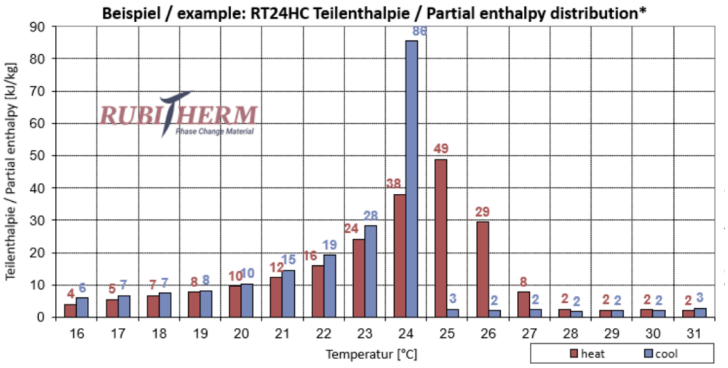

Fig. 5. Enthalpy vs. Temp. for RT24HC: datasheet (access verified on May '24) of *RUBITHERM*.

4.2 Thermodynamics assumptions and enthalpy-based method

The heat transfer (conduction-only) problem can written as:

$$\frac{\partial Q}{\partial t} = \nabla.(\lambda \nabla T) + \dot{q}_v \qquad \forall \mathbf{x} \in \Omega \tag{8}$$

being Q the time dependent heat of the system, λ is the thermal conductivity (which depends on temperature T and position of the considered body), $\dot{q}_v$ represents the possible source term, finally $\nabla.$ and ∇ are the divergence and gradient operators.
By introducing the definition of the enthalpy of a homogenous system, i.e., $H=U+pdV$, and by introducing the 1st thermodynamics law $dU=dQ-pdV$ (being dQ a small amount of added heat, pdV the rate of spent work and dU the variation of the system internal energy), Equation. (8) modifies into

$$\frac{\partial H}{\partial t} = \nabla.(\lambda \nabla T) + \dot{q}_v \qquad \forall \mathbf{x} \in \Omega \tag{9}$$

which is known as enthalpy-based Equation.
To solve Equation (9) the Apparent Calorific Capacity Method (ACCM) is commonly adopted for describing the enthalpy evolution of a system in terms of an apparent heat capacity during thermal phase changes. Adopting the following chain rule and introducing the so-called temperature-dependent apparent heat capacity:

$$\frac{\partial H}{\partial t} = \frac{\partial H}{\partial T}\frac{\partial T}{\partial t} \quad \text{and} \quad \frac{\partial H}{\partial T} = \rho C_{eff}(T) \tag{10}$$

Equation (10) modifies into the following non-linear ACCM transient heat Equation:

$$\rho C_{eff}(T)\frac{dT}{dt} = \nabla.(\lambda \nabla T) + \dot{q}_v \qquad \forall \mathbf{x} \in \Omega \tag{11}$$

To complete the above problem of the ACCM approach, Initial Conditions (ICs) and Boundary Conditions (BCs) need to be employed, as defined in Section 4.3.

4.3 Initial, Internal and External boundary conditions for the study cases

IC, internal and external BCs are those as shown in Fig. 6:

$$\begin{aligned} T(x,t) &= T_0 \\ \lambda \frac{\partial T}{\partial x} \cdot n &= \dot{q}_{out}(t) \quad \text{at} \quad x = 0 \quad \text{with} \quad n = -1 \\ k \frac{\partial T}{\partial x} \cdot n &= h_{\text{int}}(t)(T_{\text{int}}(t) - T_{wall\,\text{int}}(t)) \quad \text{at} \quad x = l \quad \text{with} \quad \text{n} = 1 \end{aligned} \tag{12}$$

where $\dot{q}_{\text{out}}(t)$ is the heat flux from the outside environment of the envelope, and $T_{\text{int}}(t)$ the indoor temperature. The outdoor heat flux is defined as $\dot{q}_{\text{out}}(t) = \dot{q}_{\text{rad,S}}(t) + \dot{q}_{\text{conv}}(t)$, being $\dot{q}_{\text{rad,S}}(t) = \alpha_{\text{wall}}\dot{q}_{\text{solar}}(t)$ the absorbed short-wave radiation, which depends directly on the solar absorptance α_{wall} and on the global radiation $\dot{q}_{\text{solar}}(t)$. $\dot{q}_{\text{conv}}(t)$ is the sensible heat exchanged with the environment by convection determined by means of the Newton's law of cooling $\dot{q}_{\text{conv}}(t) = h_{\text{out}}(t)[T_{\text{out}}(t) - T_{\text{wallout}}(t)]$, with $h_{\text{out}}(t)$ the outdoor convective transfer coefficient, $T_{\text{out}}(t)$ the outdoor temperature, and $T_{\text{wallout}}(t)$ the temperature over the surface (Fig. 6). For brevity, only the west orientation has been considered in this study. A forthcoming full paper will assess all orientations, including north, east, south, and west.

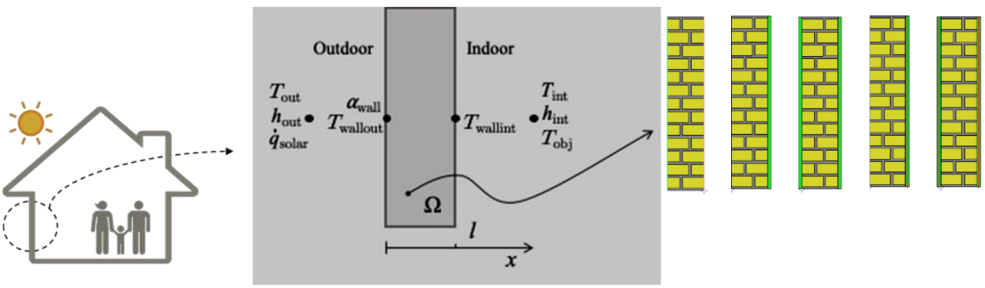

Fig. 6. Domain of analysis + boundary conditions information.

$\dot{q}_{\text{solar}}$, h_{out}, and $T_{\text{out}}$are determined by means of the typical meteorological year (TMY), which provides hourly weather data for typical meteorological months. The TMY is selected using the Sandia method from a database of weather parameters (Climate.OneBuilding repository). One location has been chosen as a case study which is Genova, Italy defined as Csb (Mediterran Climate) according to the Köppen climate classification.

5 Results and discussion of energy interventions

5.1 1D-FEM modelling results

The energy performance of the building system is analyzed at single-wall level by considering the five configurations presented in Section 4.1 and adopting the numerical approach described in Section 4.2 and 4.3.
For the transient analysis, the total time t_N was substepped into N time steps, i.e., (t_0, t_1), (t_1, t_2), ..., (t_{N-1}, t_N), with $t_0=0$. The energy performance of the different configurations was analyzed by evaluating a cost function named "C", which represents the total undesired heat loads during all the time steps of the analysis, i.e.:

$$C = \underbrace{\sum_{n=0}^{N} h_{\text{int}} \langle T_{\text{wallint}}^{(n)} - T_{\text{obj}}^{\max} \rangle}_{\text{undesired gains } C_{\text{gain}}} + \underbrace{\sum_{n=0}^{N} h_{\text{int}} \langle T_{\text{obj}}^{\min} - T_{\text{wallint}}^{(n)} \rangle}_{\text{undesired losses } C_{\text{loss}}} \tag{13}$$

where h_{int} is the indoor heat convection coefficient, $T_{\text{wallint}}^{(n)}$ is the calculated temperature over the inside the wall surface at time t_n, $T_{\text{obj}}^{\max}$ and $T_{\text{obj}}^{\min}$ are the objective indoor temperatures (maximum and minimum, respectively), and $\langle u \rangle = (u + |u|)/2$ stands for the ramp function; h_{int}, $T_{\text{obj}}^{\max}$ and are known variables of the analyses.

To define the cost function *C*, it is assumed that the indoor temperature is constant at 24 °C, thus the objective indoor temperatures are set at the same values, $T_{\text{obj}}^{\max} = T_{\text{obj}}^{\min} = 24\ ^{o}C$. It is also assumed a fixed value for the indoor convection coefficient, $h_{\text{int}} = 8.29 W/m^2/K$, and a fixed value for the solar absorptance of the outer of the envelope, $\alpha_{\text{wall}} = 0.6$. Finally, to calculate $T_{\text{wallint}}^{(n)}$ for each layer, the TES properties of the walls are those shown in Table 2. Regarding the heat transfer problem, FEM formulation is employed and for the solver a Euler-backward (implicit) time stepping is implemented. Space discretization of the envelope is made with 96 linear finite elements, while for the temporal one, a time step of 20 min.

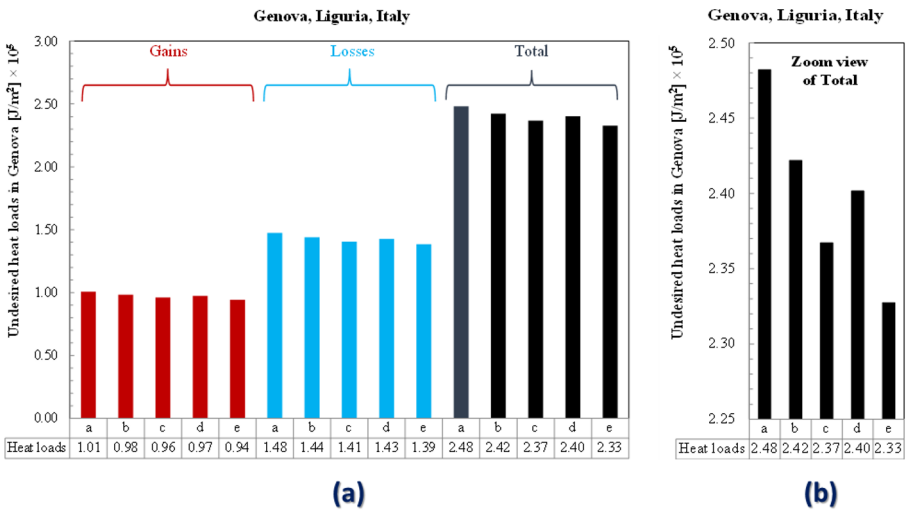

Fig. 7. Undesired heat loads for the 5 wall scenarios and considering the TMY of Genova (IT).

The total undesired heat loads (C) for the five configurations (*Scenarios a-b-c-d-e* as of Fig. 4) of Genova, Italy are shown in Fig. 7 (a) and (b), which depict the heat loads for each analyzed case. The findings of these analyses highlight that the reference walls have the highest undesired heat loads, which could result in either heat gains, losses, or overall totals. Upon analyzing the thermally retrofitted cases (i.e., the cases *b, c, d* and *e*), it can be concluded that *Scenario b* and *Scenario d* result in high undesired heat loads, while *Scenario c* and *Scenario e* demonstrate a quite good reduction in undesired heat loads (gains, losses, or totals). More specifically, *Scenario e*, which represents the URM wall retrofitted with double side with double GTRM layers which were also enhanced with PCM, performs the best performance across all cases. The reduction of the total undesired heat loads in percentage for the four retrofitted cases (Scenarios b-c-d-e) compared to URM are -2.42%, -4.63%, -3.24% and -6.23%.

5.2 Building Performance Evaluation using EnergyPlus

Let us consider the building energy simulation of the BESTEST case 900 (ANSI/ASHRAE Standard 140-2017) as case study. It represents a heavyweight building located in a flat and open terrain, having a unique thermal zone and South-exposed windows without opening nor shading. In BESTEST 900, the indoor thermal temperature is maintained between 20 and 27°C using air conditioning. Each external wall of BESTEST 900 consists of the configuration layers, thickness and material properties as presented in Section 4 (as sketched in Fig. 8).

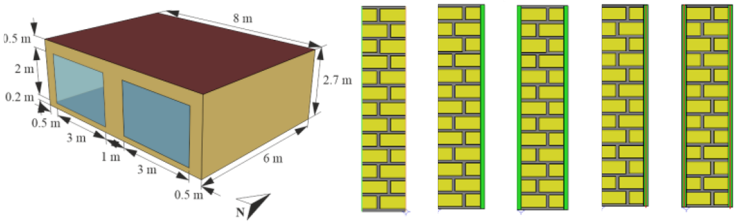

Fig. 8. Geometry of the buildings BESTEST 900 (left), and 4 layouts of their external walls (right).

The energies $\mathcal{C}$ and $\mathcal{H}$ consumed for cooling and heating, is determined using EnergyPlus™ (E⁺) V23.1.0. The input data file (*idf*) to run BESTEST 900 in E⁺ can be freely downloaded from the repository of the U.S. National Renewable Energy Laboratory (NREL) at GitHub. Besides all the building characteristics specified in the *idf*, the energy performance of a building is strongly dependent on the local weather. We assumed that the building is located at Genova-Italy, with climate Csb in the Köppen-Geiger classification, mild winter, dry summers, wet winters. To define the local weather with the detail needed for E⁺, we use the typical meteorological year (TMY) at Genova for the period 2007-2021; the corresponding E⁺ weather file (epw) is downloadable for free from (https://climate.onebuilding.org/).

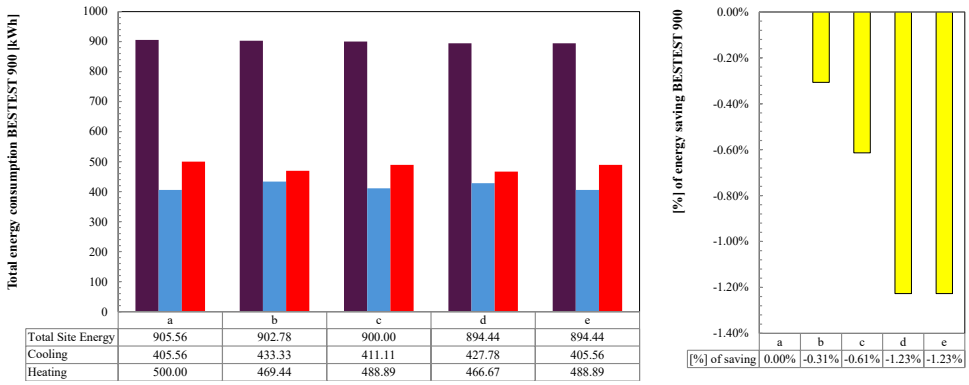

	a	b	c	d	e
Total Site Energy	905.56	902.78	900.00	894.44	894.44
Cooling	405.56	433.33	411.11	427.78	405.56
Heating	500.00	469.44	488.89	466.67	488.89

	a	b	c	d	e
[%] of saving	0.00%	-0.31%	-0.61%	-1.23%	-1.23%

Fig. 9. Annual energy consumption (cooling + heating) for the 5 wall scenarios, considering the TMY of Genova (IT) and mounted in the BESTEST 900 case; the [%] of energy saving is also disclosed.

For the five configurations of the BESTEST 900 in Genova, the annual energy consumption for cooling and heating computed by E⁺, are those plotted in Fig. 9. These analyses, as for Section 5.1, show that the URM reference walls lead to the highest annual site energy consumption of the building. Then, among the retrofitted cases, *Scenarios b* and *c* still have high energy consumption for cooling, while performing better for heating. Finally, *Scenarios d* and *e* show good energy reductions. Particularly, *Scenario e*, featuring URM walls retrofitted with double GTRM layers and enhanced with PCM, demonstrates the best energy performance. In terms of reduction percentages in total site energy consumption for

Scenarios b-e compared to URM are -0.31%, -0.61%, -1.23%, and -1.23%, respectively. Energy savings for scenarios "d" and "e" are the same because the PCM is activated only on the inside, based on its solidification and melting temperature. More effective responses can be achieved through the rational design of multi-layer systems, which will be discussed in detail in forthcoming applications and future papers.

6 Conclusions

This work deals with the integration of seismic and energy retrofitting of masonry elements strengthened with PCM-enhanced GTRM/FRCM systems. It demonstrated potential novelty for improving the resilience and sustainability of (new and existing) buildings, particularly in regions like Italy where UnReinforced Masonry (URM) walls are prevalent. By combining seismic strengthening with energy efficiency techniques through innovative materials like Phase Change Materials (PCMs), this study offers a novel approach to retrofit aging structures. The optimized design framework not only enhances the shear strength and reduces the seismic vulnerability of the analyzed walls but also improves their thermal energy performance, leading to significant savings for heating and cooling. This integrated strategy ensures that retrofitted buildings achieve high structural integrity while maintaining optimal indoor thermal comfort, representing a significant step forward in sustainable construction. Future developments of the research are addressed to consider the integration of two aspects in a synergic way in the design phase solving a non-linear constrained optimization problem, where the objective function is a coupled mechanical-based performance mixed with the energy consumption for cooling and heating.

Acknowledgments: We sincerely thank the European Commission for its support and funding through the Marie Skodowska-Curie Actions (MSCA) scheme under Grant Agreement ID: 101086440, which made the BEST (Bio-based Energy-efficient materials and Structures for Tomorrow) project possible. This research is also part of the research activities of the WP5 - “Integrated, low-impact and rapid retrofit interventions” (coord. Prof. F. da Porto and Prof. A. Prota) within DPC-ReLUIS 2022-2024 projects funded by the Dipartimento della Protezione Civile, Italy. The opinions expressed in this publication are those of the authors and are not necessarily endorsed by the Dip. della Protezione Civile.

References

1. D. A. Pohoryles, D. A. Bournas, F. Da Porto, A. Caprino, G. Santarsiero, and T. Triantafillou, Integrated seismic and energy retrofitting of existing buildings: A state-of-the-art review. J. Build. Eng. **61**, 105274 (2022). https://doi.org/10.1016/j.jobe.2022.105274
2. M. Economidou, B. Atanasiu, C. Despret, J. Maio, I. Nolte, and O. Rapf, Europe’s buildings under the microscope – a country-by-country review of the energy performance of buildings. Brussels: Buildings Performance Institute Europe; Bpie 35 (2011)
3. A. Marini, C. Passoni, A. Belleri, F. Feroldi, M. Preti, G. Metelli, P. Riva, E. Giuriani, and G. Plizzari, Combining seismic retrofit with energy refurbishment for the sustainable renovation of RC buildings: a proof of concept. Eur. J. Environ. Civ. Eng. **26**, 2475 (2022). https://doi.org/10.1080/19648189.2017.1363665
4. G. M. Calvi, L. Sousa, and C. Ruggeri, Energy Efficiency and Seismic Resilience: A Common Approach. in *Multi-Hazard Approaches to Civ. Infrastruct. Eng.* (Springer International Publishing, Cham, 2016), pp. 165–208. https://doi.org/10.1007/978-3-319-29713-2_9

5. T. C. Guimarães, O. da F. M. Gomes, O. M. Oliveira de Araújo, R. Tadeu Lopes, M. Y. R. Da-Gloria, R. D. Toledo Filho, E. Koenders, A. Caggiano, C. Mankel, M. Nazari Sam, R. G. Mendes de Andrade, and S. R. Ferreira, PCM-Impregnated Textile-Reinforced Cementitious Composite for Thermal Energy Storage. Textiles **3**, 98 (2023). https://doi.org/10.3390/textiles3010008
6. D. A. Bournas, Concurrent seismic and energy retrofitting of RC and masonry building envelopes using inorganic textile-based composites combined with insulation materials: A new concept. Compos. Part B Eng. **148**, 166 (2018). https://doi.org/10.1016/j.compositesb.2018.04.002
7. C. Menna, L. Felicioni, P. Negro, A. Lupíšek, E. Romano, A. Prota, and P. Hájek, Review of methods for the combined assessment of seismic resilience and energy efficiency towards sustainable retrofitting of existing European buildings. Sustain. Cities Soc. **77**, 103556 (2022). https://doi.org/10.1016/j.scs.2021.103556
8. E. Baek, D. A. Pohoryles, S. Kallioras, D. A. Bournas, H. Choi, and T. Kim, Innovative seismic and energy retrofitting of wall envelopes using prefabricated textile-reinforced concrete panels with an embedded capillary tube system. Eng. Struct. **265**, 114453 (2022). https://doi.org/10.1016/j.engstruct.2022.114453
9. V. D. Fachinotti, F. Bre, C. Mankel, E. A. B. Koenders, and A. Caggiano, Optimization of Multilayered Walls for Building Envelopes Including PCM-Based Composites. Materials (Basel). **13**, 2787 (2020). https://doi.org/10.3390/ma13122787
10. M. Sam, A. Caggiano, L. Dubyey, J.-L. Dauvergne, and E. Koenders, Thermo-physical and mechanical investigation of cementitious composites enhanced with microencapsulated phase change materials for thermal energy storage. Constr. Build. Mater. **340**, 127585 (2022). https://doi.org/10.1016/j.conbuildmat.2022.127585
11. C. Mankel, A. Caggiano, and E. Koenders, Thermal energy storage characterization of cementitious composites made with recycled brick aggregates containing PCM. Energy Build. **202**, 109395 (2019). https://doi.org/10.1016/j.enbuild.2019.109395
12. I. Peralta, V. D. Fachinotti, E. A. B. Koenders, and A. Caggiano, Computational design of a Massive Solar-Thermal Collector enhanced with Phase Change Materials. Energy Build. **274**, 112437 (2022). https://doi.org/10.1016/j.enbuild.2022.112437
13. Y. A. Al-Salloum, N. A. Siddiqui, H. M. Elsanadedy, A. A. Abadel, and M. A. Aqel, Textile-Reinforced Mortar versus FRP as Strengthening Material for Seismically Deficient RC Beam-Column Joints. J. Compos. Constr. **15**, 920 (2011). https://doi.org/10.1061/(ASCE)CC.1943-5614.0000222
14. C. Papanicolaou, T. Triantafillou, and M. Lekka, Externally bonded grids as strengthening and seismic retrofitting materials of masonry panels. Constr. Build. Mater. **25**, 504 (2011). https://doi.org/10.1016/j.conbuildmat.2010.07.018
15. M. Ponte, A. Penna, and R. Bento, In-plane cyclic tests of strengthened rubble stone masonry. Mater. Struct. **56**, 41 (2023). https://doi.org/10.1617/s11527-023-02126-8
16. J. Donnini, V. Corinaldesi, and A. Nanni, FRCM Mechanical Properties Using Carbon Fabrics With Different Coating Treatments. in *SP-305 Durab. Sustain. Concr. Struct.* (American Concrete Institute, 2015), pp. 8.1-8.12. https://doi.org/10.14359/51688568
17. D. A. Bournas, P. V. Lontou, C. G. Papanicolaou, and T. C. Triantafillou, Textile-Reinforced Mortar versus Fiber-Reinforced Polymer Confinement in Reinforced Concrete Columns. ACI Struct. J. **104**, 740 (2007). https://doi.org/10.14359/18956
18. L. N. Koutas, Z. Tetta, D. A. Bournas, and T. C. Triantafillou, Strengthening of Concrete Structures with Textile Reinforced Mortars: State-of-the-Art Review. J.

Compos. Constr. **23**, 3118001 (2019). https://doi.org/10.1061/(ASCE)CC.1943-5614.0000882

19. D. A. Bournas and T. C. Triantafillou, Investigation of Bar Buckling in Columns Confined with Composite Material Jackets. in *SP-275 Fiber-Reinforced Polym. Reinf. Concr. Struct. 10th Int. Symp.* (American Concrete Institute, 2011), pp. 117–134. https://doi.org/10.14359/51682417
20. T. C. Triantafillou and C. G. Papanicolaou, Shear strengthening of reinforced concrete members with textile reinforced mortar (TRM) jackets. Mater. Struct. Constr. **39**, 93 (2006). https://doi.org/10.1617/s11527-005-9034-3
21. S. M. Raoof and D. A. Bournas, TRM versus FRP in flexural strengthening of RC beams: Behaviour at high temperatures. Constr. Build. Mater. **154**, 424 (2017). https://doi.org/10.1016/j.conbuildmat.2017.07.195
22. C. Menna, C. Del Vecchio, M. Di Ludovico, G. M. Mauro, F. Ascione, and A. Prota, Conceptual design of integrated seismic and energy retrofit interventions. J. Build. Eng. **38**, 102190 (2021). https://doi.org/10.1016/j.jobe.2021.102190
23. A. Furtado, A. Arêde, and H. Rodrigues, The Effect of a Textile-Reinforced Mortar on the Flexural Response of Energy-Improved Infill Walls. J. Compos. Constr. **26**, 4022047 (2022). https://doi.org/10.1061/(ASCE)CC.1943-5614.0001237
24. P. Gkournelos and T. Triantafillou, Integrated Structural and Energy Retrofitting of Masonry Walls: The Effect of In-Plane Damage on the Out-Of-Plane Response. in *Lect. Notes Civ. Eng.* (American Society of Civil Engineers, 2022), pp. 1819–1836. https://doi.org/10.1007/978-3-030-88166-5_157
25. L. Mercedes, E. Bernat-Maso, and L. Gil, In-plane cyclic loading of masonry walls strengthened by vegetal-fabric-reinforced cementitious matrix (FRCM) composites. Eng. Struct. **221**, 111097 (2020). https://doi.org/10.1016/j.engstruct.2020.111097
26. L. A. S. Kouris and T. C. Triantafillou, State-of-the-art on strengthening of masonry structures with textile reinforced mortar (TRM). Constr. Build. Mater. **188**, 1221 (2018). https://doi.org/10.1016/j.conbuildmat.2018.08.039
27. C. G. Papanicolaou, T. C. Triantafillou, M. Papathanasiou, and K. Karlos, Textile reinforced mortar (TRM) versus FRP as strengthening material of URM walls: out-of-plane cyclic loading. Mater. Struct. **41**, 143 (2007). https://doi.org/10.1617/s11527-007-9226-0
28. National Research Council, Guide for the design and construction of externally bonded fibre reinforced inorganic matrix systems for strengthening existing structures. *Guide for the Design and Construction of Externally Bonded Fibre Reinforced Inorganic Matrix Systems for Strengthening Existing Structures* (2018)
29. S. Cattari and S. Lagomarsino, A strength criterion for the flexural behaviour of spandrels in un-reinforced masonry walls. in *Proc. 14th World Conf. Earthq. Eng.* (2008)
30. G. de Felice, S. De Santis, L. Garmendia, B. Ghiassi, P. Larrinaga, P. B. Lourenço, D. V. Oliveira, F. Paolacci, and C. G. Papanicolaou, Mortar-based systems for externally bonded strengthening of masonry. Mater. Struct. **47**, 2021 (2014). https://doi.org/10.1617/s11527-014-0360-1
31. A. Bilotta, F. Ceroni, E. Nigro, and M. Pecce, Experimental tests on FRCM strengthening systems for tuff masonry elements. Constr. Build. Mater. **138**, 114 (2017). https://doi.org/10.1016/j.conbuildmat.2017.01.124
32. ACI 549-L Committee and RILEM TC 250-CSM, Guide to Design and Construction of Externally Bonded Fabric-Reinforced Cementitious Matrix (FRCM) and Steel-

Reinforced Grout (SRG) Systems for Repair and Strengthening Masonry Structures. *Guide to Design and Construction of Externally Bonded Fabric-Reinforced Cementitious Matrix (FRCM) and Steel-Reinforced Grout (SRG) Systems for Repair and Strengthening Masonry Structures* (2020)

33. NTC18 Ministero delle Infrastrutture e dei Trasporti, Aggiornamento delle Norme tecniche per le costruzioni (in Italian); https://www.gazzettaufficiale.it/eli/gu/2018/02/20/42/so/8/sg/pdf. *Aggiornamento Delle Norme Tecniche per Le Costruzioni (in Italian); Https://Www.Gazzettaufficiale.It/Eli/Gu/2018/02/20/42/so/8/Sg/Pdf* (2018)
34. V. Turnšek and F. Čačovič, Some experimental results on the strength of brick masonry walls. in *Proc. 2nd Int. Brick Mason. Conf.* (British Ceramic Research Association Stoke-on-Trent, UK, 1971), pp. 149–156
35. National Research Council, CNR-DT 212/2013. Instructions for the Reliability Assessment of Seismic Safety of Existing Buildings, National Research Council, Rome (in italian). *CNR-DT 212/2013. Instructions for the Reliability Assessment of Seismic Safety of Existing Buildings, National Research Council, Rome (in Italian).* (2013)
36. G. Grünthal, European Macroseismic Scale 1998. Eur. Cent. Geodyn. … **15**, 100 (1998)
37. S. Babaeidarabad, D. Arboleda, G. Loreto, and A. Nanni, Shear strengthening of un-reinforced concrete masonry walls with fabric-reinforced-cementitious-matrix. Constr. Build. Mater. **65**, 243 (2014). https://doi.org/10.1016/j.conbuildmat.2014.04.116
38. S. Babaeidarabad and A. Nanni, URM walls strengthened with fabric-reinforced cementitious matrix (FRCM) subjected to in-plane and out-of-plane load. Proc. 7th Int. Conf. FRP Compos. Civ. Eng. CICE 2014 **18**, 4013045 (2014)
39. G. P. Lignola, A. Prota, and G. Manfredi, Numerical simulations of in-plane behavior of tuff masonry strengthened with cementitious matrix-grid composites. Proc. 1st Asia-Pacific Conf. FRP Struct. APFIS 2007 **1**, 255 (2007)
40. F. Parisi, I. Iovinella, A. Balsamo, N. Augenti, and A. Prota, In-plane behaviour of tuff masonry strengthened with inorganic matrix-grid composites in diagonal compression. ECCM 2012 - Compos. Venice, Proc. 15th Eur. Conf. Compos. Mater. **45**, 1657 (2012)
41. G. Marcari, M. Basili, and F. Vestroni, Experimental investigation of tuff masonry panels reinforced with surface bonded basalt textile-reinforced mortar. Compos. Part B Eng. **108**, 131 (2017). https://doi.org/10.1016/j.compositesb.2016.09.094